# A filtration model applied to submerged anaerobic MBRs (SAnMBRs)

A. Robles[a,*], M.V. Ruano[b], J. Ribes[b], A. Seco[b] and J. Ferrer[a]

[a] Institut Universitari d'Investigació d'Enginyeria de l'Aigua i Medi Ambient, IIAMA, Universitat Politècnica de València, Camí de Vera s/n, 46022 Valencia, Spain (e-mail: *ngerobma@upv.es; jferrer@hma.upv.es*)

[b] Departament d'Enginyeria Química, Escola Tècnica Superior d'Enginyeria, Universitat de València, Avinguda de la Universitat s/n, 46100 Burjassot, Valencia, Spain (e-mail: *m.victoria.ruano@uv.es; josep.ribes@uv.es; aurora.seco@uv.es)*

* Corresponding author: tel. +34 96 387 99 61, fax +34 96 387 90 09, e-mail: *ngerobma@upv.es*

**Abstract**

The aim of this study was to develop a model able to correctly reproduce the filtration process of submerged anaerobic MBRs (SAnMBRs). The proposed model was calibrated and validated in a SAnMBR demonstration plant fitted with industrial-scale hollow-fibre membranes. Three suspended components were contemplated in the model: total solids concentration; dry mass of cake on the membrane surface; and dry mass of irreversible fouling on the membrane surface. The model addressed the following physical processes: the build-up and compression of the cake layer during filtration; cake layer removal using biogas sparging to scour the membrane; cake layer removal during back-flushing; and the consolidation of irreversible fouling. The short- and long-term validation of the model resulted in correlation coefficients ($R^2$) of 0.962 and 0.929, respectively.

**Keywords**

Industrial-scale hollow-fibre membranes; resistance-in-series-based; filtration model; submerged anaerobic MBR

**Highlights**

A model for filtration in SAnMBRs has been developed.

This model (based on the resistance-in-series model) can easily be used with any biological model.

The model was calibrated and validated using industrial-scale hollow-fibre membranes.

Short- and long-term validation resulted in $R^2$ of 0.962 and 0.929, respectively.

**Graphical abstract**

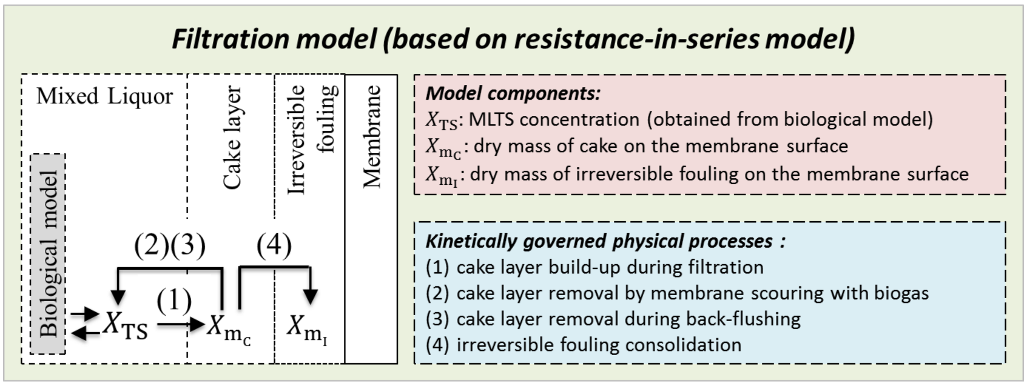


## 1. Introduction

In recent years, membrane bioreactors (MBRs), particularly submerged versions [1], have attracted a lot of attention in the realm of wastewater treatment. Rather than aerobic MBRs, submerged anaerobic MBRs (SAnMBR) have emerged as a promising technology for municipal wastewater treatment because not only do they feature the main advantages of MBRs (i.e. clarified and partially disinfected effluent and a smaller environmental footprint for WWTPs) but they also offer the greater sustainability of anaerobic rather than aerobic processes, i.e. low sludge production (due to low anaerobic biomass yield), low energy consumption (no aeration required) and, finally, the biogas generated can be used as an energy resource.

However, further study of membrane technology is needed in order to gain more insight into how to optimise their efficiency. One key operating challenge of SAnMBR technology in particular concerns how membrane performance can be optimised whilst minimising membrane fouling. In this respect, mathematical modelling of MBR technology may help provide an insight into the factors that play a key role in membrane fouling [1], whilst providing invaluable data for the design, forecast and control of membrane technology [2].

The biological processes involved in MBR systems can be successfully modelled by using either classical models [3, 4] or plant-wide models [5, 6].

As for the modelling of the physical processes (in addition to the modelling of integrated processes, i.e. biological + physical processes), several empirical/semi-empirical models have been proposed [7, 8, 9] to express the relationship between sludge characteristics and/or operating conditions, and membrane fouling. Broekmann et al. [10] modelled the pore blocking and cake formation in membrane filtration taking into account the adhesive forces between the particles and the membrane surface, and also the impact of the particle and membrane pore size distributions. Duclos-Orsello et al. [11] proposed a model for the decrease in flux during microfiltration (as a function of the bulk solids concentration) using three classical fouling mechanisms: pore blockage, pore constriction and cake formation. Li and Wang [12] proposed a “comprehensive mathematical model for membrane fouling in a submerged MBR” that includes the impact of shear intensity on membrane scouring. Brusch et al. [13] created a model of submerged hollow-fibre (HF) membrane filtration that incorporated the geometry and hydrodynamics of the system. Zarragoitia-González et al. [14] developed a mathematical model for simulating the filtration process and impact of aeration in submerged MBRs, including biological kinetics and the dynamics of sludge build-up on membranes and its removal by the formation and degradation of soluble microbial products (SMP). Mannina et al. [1] proposed an advanced model for MBR systems that takes into account the exchange of mixed liquor total solids (MLTS) and SMP between mixed liquor and membrane surface. Wu et al. [15] modelled membrane fouling in a submerged MBR by considering the role of MLTS, soluble and colloidal components, activated sludge floc distribution and aeration intensity.

Most of the above-mentioned modelling approaches can reproduce the way in which sludge affects membrane performance. However, these models usually rely on parameters that cannot be measured on line and require specific laboratory equipment (e.g. SMP). Moreover, some of them cannot reproduce the impact of the different membrane module operating stages (relaxation, back-flushing…) or cannot easily be used together with a given biological model. In this respect, some authors are currently developing simple new filtration models that can easily be used in conjunction with biological processes in an attempt to reproduce the impact of the most critical fouling variables, i.e. membrane tank shear intensity and MLTS. For instance, Ludwig et al. [16] proposed a dynamic model for simulating submerged membranes on the basis of the standard parameters usually measured in filtration processes (MLTS and cross flow aeration); whilst Sarioglu et al. [17] proposed a “resistance-in-series” membrane filtration model that considers overall membrane resistance in terms of three distinct components: intrinsic membrane resistance, accumulated solids resistance and membrane fouling resistance.

The main objective of our study, based on said resistance-in-series filtration model, is to propose a filtration model able to correctly reproduce the filtration performance of SAnMBR technology. On the basis of the experimental results obtained whilst operating a SAnMBR plant fitted with industrial-scale HF membranes, we developed, calibrated and validated a filtration model (based on the resistance-in-series model) that can easily be used in conjunction with a biological model. The model proposed takes into account the effect of the shear intensity in the membrane tank caused by the flow of recycled biogas. This makes it possible to reproduce the membrane scouring process occurring during the different membrane module operating stages (filtration, relaxation…). The physical processes contemplated in our model are: cake layer build-up and compression during filtration; cake layer removal using biogas sparging to scour the membrane; cake layer removal during back-flushing; and the consolidation of irreversible fouling.

## 2. Materials and methods

### *2.1. SAnMBR plant description*

The filtration model proposed in our study was calibrated and validated using data obtained from a demonstration-scale SAnMBR system. The plant consists of an anaerobic reactor with a total volume of 1.3 $m^3$ (0.4 $m^3$ head space for biogas) connected to two membrane tanks each with a total volume of 0.8 $m^3$ (0.2 $m^3$ head space for biogas). Each membrane tank (MT) has one industrial HF ultrafiltration membrane unit (PURON®, Koch Membrane Systems (PUR-PSH31) with 0.05 µm pores). Each module has a total membrane surface of 30 $m^2$. To recover the bubbles of biogas in the permeate leaving the membrane tank, two degasification vessels (DV) were installed: one between each MT and the respective vacuum pump. The funnel-shaped section of conduit makes the biogas accumulate at the top of the DV. The resulting permeate is stored in the CIP tank.

Complete stirring conditions are assumed in the anaerobic reactor and the MTs. To provide proper stirring conditions in the anaerobic reactor, a portion of the sludge is continuously pumped from bottom to top. In addition, a fraction of the produced biogas is recycled from its bottom to improve the stirring conditions. On the other hand, the sludge is continuously recycled from the anaerobic reactor through the external MTs. Another fraction of the produced biogas is also recycled to the MTs from the bottom of each fibre bundle, which improves the stirring conditions.

The membrane operating schedule included not only the classic membrane operating stages (filtration, relaxation and back-flushing) but also a ventilation stage. In the ventilation stage, permeate is pumped into the membrane tank through the degasification vessel instead of through the membrane. The aim of ventilation is to recover the biogas that accumulates in the degasification vessel. As regards membrane cleaning, ventilation acts as relaxation since no transmembrane flux is applied whilst maintaining a given gas sparging intensity.

For further details of this SAnMBR system, see Robles et al. [18].

*2.2. Monitoring system*

Many on-line sensors and automatic devices were installed in order to automate and control plant operations and provide on-line information about the state of the process. The on-line sensors used in this study were: 1 solids concentration sensor located in the anaerobic reactor; 1 flow indicator transmitter for the permeate pump; 1 flow indicator transmitter for the membrane tank blower; 1 pH-temperature sensor located in the membrane tank; and 1 liquid pressure indicator transmitter to monitor the transmembrane pressure (TMP). The actuators used in this study were: 1 group of on/off flow-direction valves to control the different membrane operating stages (filtration, back-flushing, ventilation…), and 2 frequency converters to control the rotating speed of the permeate pump and the membrane tank blower.

In addition to being monitored on line, grab samples of anaerobic sludge were taken once a day to assess filtration performance. MLTS was determined according to Standard Methods [19] using procedure 2540 B. Influent COD was also daily determined by Standard Methods [19].

## 3. Description of model

Our proposed model was developed on the basis of the resistance-in-series model using the experimental results obtained from operating a SAnMBR plant fitted with industrial-scale HF membranes. Our model contemplates two parameters usually measured in filtration processes: MLTS and biogas recycling flow. Although MLTS is an elementary parameter in comparison with the complexity of the model, MLTS was defined as model input because it can be directly linked with the existing biological models and it is easy to measure. This model reproduces the main processes that occur during filtration in SAnMBRs: cake layer build-up and consolidation during filtration; membrane scouring by biogas sparging; removal of cake layer by back-flushing; and irreversible fouling consolidation. MLTS and biogas recycling flow were identified as the key model parameters related to cake layer build-up and membrane scouring by biogas sparging. In this regard, MLTS and biogas recycling flow finally determine the dry mass of cake on the membrane surface. This was established on the basis of the experimental results obtained from different flux-step trials conducted throughout the whole operating period of the plant. On the other hand, the irreversible fouling consolidation process was considered as a function not only of the dry mass of solids forming the cake-layer but also function of an irreversible fouling rate constant. This irreversible fouling rate constant indirectly reflects the possible effect of the different bulk characteristics affecting the physiological state of the biomass thus affecting the irreversible fouling phenomenon, such as, for instance, EPSs and SMPs composition.

### *3.1. Conceptual modelling*

#### *3.1.1. Resistance-in-series model*

The proposed filtration model is based on the resistance-in-series model. The resistance-in-series model (Eq. 1) describes the flux through each in-series medium using Darcy's law: the permeate volume ($V$, $m^3$) is driven through each medium by a difference in transmembrane hydraulic pressure and the total filtration resistance ($R_T$, $m^{-1}$) is assumed to be the sum of the different assumed partial resistances.

$$J = \frac{1}{A}\frac{dV}{dt} = \frac{TMP}{\mu \cdot R_T} \quad \text{(Eq. 1)}$$

Like other authors [16, 17], our model contemplates the following three partial resistances (Eq. 2): cake layer resistance ($R_C$, $m^{-1}$); irreversible fouling resistance ($R_I$, $m^{-1}$); and intrinsic membrane resistance ($R_M$, $m^{-1}$). Taking into account the membrane operating mode, cake build-up was considered to be the main fouling mechanism in the short-term, and irreversible fouling, the main fouling mechanism in the long-term. Therefore, the model must be calibrated correctly not only in the short term but also in the long term.

$$R_T = R_C + R_I + R_M \qquad \text{(Eq. 2)}$$

As regards $R_C$, Sarioglu et al. [17] assumed the cake layer to be homogenous, making it possible to calculate the cake layer thickness ($\delta_C$) using Eq. 3.

$$\delta_C = \frac{m_c}{\rho_c \cdot (1-\varepsilon) \cdot A} \qquad \text{(Eq. 3)}$$

Where:

- $m_c$ is the dry mass of cake layer (kg).
- $\rho_c$ is the cake density (kg m$^{-3}$).
- $A$ is the area of the medium (m$^2$).
- $\varepsilon$ is the porosity (dimensionless) $= \frac{Total\ pores\ volume}{Total\ porous\ media\ volume}$

Defining the coefficient $m_c/A$ as $\omega_C$ (the mass of cake deposited per membrane area, kg m$^{-2}$), redefines the cake layer thickness thus (Eq. 4):

$$\delta_C = \frac{\omega_C}{\rho_c \cdot (1-\varepsilon)} \qquad \text{(Eq. 4)}$$

On the other hand, $R_C$ can be calculated by combining the cake layer thickness equation and the Carman-Kozeny equation for flow through porous passages as follows [17]:

$$R_C = 180\frac{(1-\varepsilon)\cdot \omega_C}{\varepsilon^3 \cdot d_p^2 \cdot \rho_c} \qquad \text{(Eq. 5)}$$

Where:

- $d_p$ is the pore diameter ($m^2$).

From Eq. 5 we define the average specific cake resistance ($\alpha_C$, m $kg^{-1}$) as shown in Eq. 6 and $R_C$ can be expressed as shown in Eq. 7.

$$\alpha_C = \frac{180\cdot(1-\varepsilon)}{\varepsilon^3 \cdot d_p^2 \cdot \rho_c} \qquad \text{(Eq. 6)}$$

$$R_C = \omega_C \cdot \alpha_C \qquad \text{(Eq. 7)}$$

Concerning $R_I$, the same approach than the one used for defining $\alpha_C$ and $\omega_C$ was considered for defining the average specific irreversible fouling resistance ($\alpha_I$, m $kg^{-1}$) and the mass of irreversible fouling per membrane area ($\omega_I$, kg $m^{-2}$). Therefore, assuming $R_M$ to be constant over time, the resistance-in-series model shown in Eq. 1 can be assumed to represent the dynamic evolution of TMP as shown in Eq. 8.

$$TMP\ (t) = J \cdot \mu \cdot (\omega_C \cdot \alpha_C + \omega_I \cdot \alpha_I + R_M) \qquad \text{(Eq. 8)}$$

Defining the average specific resistances allows reducing a great deal of effort related to correctly determine specific characteristics of the filter medium that Carman-Kozeny equation requires. It is, therefore, advisable to minimise the number of parameters to be included in the model.

The value of $\alpha_C$ was assumed to be time and TMP dependent (its calibration protocol is shown in following sections).

*3.2. Cake layer compression and sub-critical fouling*

As per the methodology proposed by Bugge et al. [20] and Jørgensen et al. [21], a linear relationship was assumed between the specific resistance of the cake and TMP (see Eq. 9).

$$\alpha_{C,TMP} = \alpha_{C,0} \cdot \left(1 + \frac{TMP}{TMP_a}\right) \qquad \text{(Eq. 9)}$$

Where:

- $\alpha_{C,TMP}$ is the specific resistance of the cake at the operating TMP (kg m$^{-2}$).
- $\alpha_{C,0}$ is the specific resistance of the cake at zero pressure (kg m$^{-2}$).
- $TMP_a$ is the pressure needed to double the specific resistance (Pa).

On the other hand, cake compression caused by a drop in pressure is time dependent due to both the deformation of soft sludge flocs and the structural rearrangement of particles [23]. The increase in the specific resistance of the cake as a result of the pressure drop over time is described in Eq. 10.

$$\frac{d\alpha_C}{dt} = k_t \cdot \left(\alpha_{C,TMP} - \alpha_C\right) \qquad \text{(Eq. 10)}$$

Where:

- $\frac{d\alpha_C}{dt}$ is the change in $\alpha_C$ (kg m$^{-2}$).
- $dt$ is the time step (s).
- $k_t$ is the time constant (s$^{-1}$).
- $\alpha_C$ is the specific resistance of the cake (kg m$^{-2}$).

Eq. 11 shows the Euler solution (using the Backward Euler Method) to Eq. 10.

$$\alpha_C(t) = \alpha_C(t - dt) + k_t \cdot \left(\alpha_{C,TMP} - \alpha_C\,(t - dt)\right) \cdot dt \qquad \text{(Eq. 11)}$$

Where:

- $\alpha_C(t)$ is the specific resistance of the cake at time t (kg $m^{-2}$).
- $\alpha_C(t - dt)$ is the specific resistance of the cake at a previous moment in time (kg $m^{-2}$).

In our study, setting the maximum time step size to 10 seconds was enough to minimise the numerical error. Moreover, the time step must be maintained at low levels to properly reproduce the effect of the different operating stages (i.e. filtration, back-flushing, etc.) on membrane performance.

On the other hand, the overall filtration resistance was seen to increase (even when operating sub-critically) during extended filtration periods. This was attributed mainly to increasing partial resistances, not contemplated in the model, associated with specific fouling mechanisms such as colloidal matter absorption. In this respect, Hughes and Field [24] observed that colloidal matter absorption increases the specific resistance of cake-like deposits, as a result of which their impact is greater than it would be without such absorption. Therefore, we incorporated an additional single dependence of $\alpha_C$ on time (see Eq. 12).

$$\alpha_C(t) = \alpha_C(t - dt) + k_{SF} \cdot dt \qquad \text{(Eq. 12)}$$

Where:

- $k_{SF}$ is the sub-critical fouling parameter (kg m$^{-2}$ s$^{-1}$).

In our model, we propose that Eq. 11 (dependence of cake compression on TMP and time) be combined with Eq. 12 (dependence of sub-critical fouling on time) to give the final variation in $\alpha_C$ (see Eq. 13). Therefore, when the maximum $\alpha_C$ related to the structural rearrangement of particles is reached at a given TMP, it is possible to account for the increase in $\alpha_C$ due to the absorption of colloids.

$$\alpha_C(t) = \alpha_C(t-dt) + \max\left(k_{SF},\ k_t \cdot \left(\alpha_{C,TMP} - \alpha_C\,(t-dt)\right)\right) \cdot dt \qquad \text{(Eq. 13)}$$

*3.3. Modelling approach*

We propose a black-box approach to describe the most important physical interactions occurring in fouling: the attachment of solids to the membrane surface; the removal of solids from the membrane surface; and the irreversible fouling of the membrane. Stirring is considered to be complete, therefore uniform MLTS and shear conditions are assumed. The notation used in this modelling approach complies with the nomenclature proposed by Corominas et al. [25] and the Petersen/Gujer matrix structure.

The model contemplates 3 suspended components:

$X_{\mathrm{TS}}$ [kg TS m$^{-3}$] is the MLTS concentration (this component can be obtained from the biological model).

$X_{\mathrm{m_C}}$ [kg TS] is the dry mass of cake on the membrane surface.

$X_{\mathrm{m_I}}$ [kg TS] is the dry mass of irreversible fouling on the membrane surface.

The model we developed contemplates a total of four kinetically governed physical processes: (1) cake layer build-up during filtration; (2) cake layer removal using biogas sparging to scour the membrane; (3) cake layer removal during back-flushing; and (4) irreversible fouling consolidation. Table 1 shows the stoichiometry of these four processes. The model does not consider diffusive back transport as this process is thought to be less significant than the other processes considered [16].

Table 2 shows the conversion factors to be applied to the elements of the model in the continuity equations. Since no biological processes are contemplated in relation to the cake layer, a value of 1 was assigned to the yield of $X_{\mathrm{m_I}}$ generated from $X_{\mathrm{m_C}}$. However, this parameter could be calculated by taking into account the actual content of the bulk foulants that contribute to irreversible fouling (i.e. $i_{\mathrm{TS}\_X_{\mathrm{m_I}}}$ in Table 2).

Table 3 shows the kinetic expressions of the processes included in the model. Process 1 (cake layer build-up) is the convective transport of foulants ($X_{\mathrm{TS}}$ in the model) to the membrane, which is a function of the permeate flow-rate ($Q_{20P}$) and the bulk concentration ($X_{\mathrm{TS}}$). Process 2 (membrane scouring by biogas sparging) is the impact of the hydrodynamic conditions in the membrane tank caused by biogas sparging (measured as $\mathrm{BRF_V}$: biogas recycling flow per bulk volume in the membrane tank). In our study, a maximum membrane scouring velocity ($q_{\mathrm{MS,Max}}$) was defined for process 2. In process 3, the back-flushing removal rate is defined as a function of the back-flushing flow rate ($Q_{20BF}$) and $X_{\mathrm{m_C}}$. Like Sarioglu et al. [17], we defined a maximum back-flushing removal velocity ($q_{\mathrm{BF,Max}}$) for process 3.

One half-saturation switching function ($M_{\mathrm{Xm_C}}$, Eq. 14) for both membrane scouring (process 2) and back-flushing (process 3) was used to vary the removal of solids smoothly as the cake layer disappeared [17].

$$M_{X_{\mathrm{m_C}}} = \frac{X_{\mathrm{m_C}}}{K_{S,X_{\mathrm{m_C}}} + X_{\mathrm{m_C}}} \qquad \text{(Eq. 14)}$$

Where:

- $K_{S,\mathrm{Xm_C}}$ is the half-saturation coefficient for the mass of cake solids during membrane scouring and back-flushing (kg TS).

On the basis of the results obtained from different flux-step trials conducted in accordance with Robles et al. [26], a fouling rate (FR) model was defined as a function of $BRF_V$ and MLTS (see Eq. 15).

$$FR = K_F \cdot e^{\left(J_{20} \cdot (\beta_1 \cdot BRF_V + \beta_2 \cdot MLTS + \gamma)\right)} \qquad \text{(Eq. 15)}$$

Where:

- $K_F$ is the adjustment parameter representing the fouling rate when the gross 20 ºC-normalised transmembrane flux ($J_{20}$) tends to zero (Pa $s^{-1}$).
- $\beta_1$, $\beta_2$, $\gamma$ are the model parameters ([$s^2$ $m^{-1}$], [s $m^2$ $kg^{-1}$] and [s $m^{-1}$], respectively).

Eq. 15 predicts that when the membranes are operated sub-critically at given operating conditions ($BRF_V$ and MLTS), the value of FR remain low, which implies operating at maximum membrane scouring velocity ($q_{\mathrm{MS,Max}}$). On the other hand, a considerable increase in FR is observed when operating supra-critically, which implies a reduction in the membrane scouring rate ($q_{MS}$). Therefore, one sigmoid inhibition function ($I_{MS}$, Eq. 16) was defined and used in process 2 to model the impact of filtering at conditions above or below critical levels.

$$I_{MS} = \frac{1}{1+FR} = \frac{1}{1+K_F \cdot e^{\left(J_{20} \cdot \left(\beta_1 \cdot BRF_V + \beta_2 \cdot MLTS + \gamma\right)\right)}} \qquad \text{(Eq. 16)}$$

Moreover, on the basis of long-term experimental results, the value of $\gamma$ was defined as a function of $R_I$ to account for the reduction over time in the filtering capacity of the membranes due to the onset of irreversible fouling. This dependence on irreversible fouling can be expressed as:

$$\gamma_t = \gamma_0 - \left(R_{I_t} - R_{I_0}\right) \cdot k_{RI} \qquad \text{(Eq. 17)}$$

Where:

- $\gamma_t$ is the value of $\gamma$ at time $t$ (s $m^{-1}$).
- $\gamma_0$ is the value of $\gamma$ at the initial time (s $m^{-1}$).
- $R_{I_t}$ is the irreversible fouling resistance at time $t$ ($m^{-1}$).
- $R_{I_0}$ is the irreversible fouling resistance at the initial time ($m^{-1}$).
- $k_{RI}$ is the proportional constant (s).

Finally, the irreversible fouling (process 4) is represented in the proposed model as a direct function of $X_{m_C}$ and a maximum irreversible fouling kinetic constant ($q_{IF,Max}$). As mentioned before, this irreversible fouling rate constant indirectly reflects the possible effect of the different bulk characteristics affecting the physiological state of the biomass thus affecting the irreversible fouling phenomenon, such as, for instance, EPSs and SMPs composition. In this regard, EPSs and SMPs seem to be the main factors affecting irreversible fouling in MBRs [27], which are directly dependent on both T [28] and SRT [29]. Commonly, SMP and EPS composition decrease as SRT increases, whilst SMP and EPS increase as T increases due to a higher microbial activity. Therefore, $q_{\mathrm{IF,Max}}$ is expected to be function of T and SRT. Nevertheless, further research is required to assess the real dependence of $q_{\mathrm{IF,Max}}$ on T and SRT and maybe to find proper link variables between biological and filtration models besides the MLTS used in this model.

## 4. Calibration of model

On the basis of the data available for estimating the parameter (dynamic measurements of TMP, MLTS and biogas recycling flow) we decided to divide the calibration procedure into the following parameter estimation subsets: off-line calibration using short-term data, dynamic calibration using short-term data, parameter estimation from experimental data, and dynamic calibration using long-term data. On the other hand, based on expert knowledge, we assigned default values to those parameters that could not be estimated from the available data.

### *4.1. Off-line calibration in the short-term*

The following parameters for membrane scouring by biogas sparging were calibrated by using the short-term filtration data obtained from different flux-step trials according to Robles et al. [26]: $K_F$, $\beta_1$, $\beta_2$ and $\gamma_0$. The FR results from the flux-step trials were adjusted to Eq. 15 using the GRG non-linear method included in the Solver complement of MS Excel. Figure 1 shows the FR results obtained in the flux-step trials conducted at three $BRF_V$ (0.0023, 0.0032 and 0.0046 $Nm^3\ h^{-1}\ m^{-3}$, equivalent to BRFs of 5, 7 and 10 $Nm^3\ h^{-1}$, respectively) and MLTS of 18.5 (Figure 1a), 22.5 (Figure 1b) and 28.5 g $L^{-1}$ (Figure 1c).

Figure 1 illustrates the different values estimated for the parameters of Eq. 15. As Figure 1 shows, it was possible to adjust $K_F$, $\beta_1$, $\beta_2$ and $\gamma_0$ to identical values for the different MLTS operating levels (18.5, 22.5 and 28.5 g $L^{-1}$). This clearly demonstrates that critical flux is dependant not only on $BRF_V$ [26] but also on MLTS.

The calibrated values of parameters $K_F$, $\beta_1$, $\beta_2$ and $\gamma_0$ included in the model are shown in Table 4.

*4.2. Dynamic calibration in the short-term*

Similar to Bugge et al. [20] and Jørgensen et al. [21], this dynamic calibration was carried out using data obtained from different flux-step trials conducted at different BRFs (5, 7 and 10 $Nm^3\ h^{-1}$) and MLTS levels (18.5, 22.5 and 28.5 g $L^{-1}$). Parameters $k_{SF}$, $\alpha_{C,0}$, $TMP_a$, and $q_{\mathrm{MS,Max}}$ related to cake build-up and compression (process 1) and membrane scouring by biogas sparging (process 2) were calibrated. The dynamic calibration consisted of adjusting the simulated TMP ($TMP_{SIM}$) to the experimental TMP ($TMP_{EXP}$). This non-linear parameter was calculated using the least squares method together with the subspace trust region method [22], based on the interior-reflective Newton method (implemented in MATLAB® LSQNONLIN), and the Runge-Kutta method (MATLAB® ode45 function). The minimising objective function (*OF*) applied is shown in Eq. 18.

$$OF = \sum \sqrt{(TMP_{SIM} - TMP_{EXP})^2} \quad \text{(Eq. 18)}$$

In this dynamic calibration, the values used for the other parameters contemplated in the proposed model are shown in Table 4 together with the values estimated for $q_{MS,Max}$, $k_{SF}$, $\alpha_{C,0}$ and $TMP_a$. It is important to emphasise that the values obtained for $\alpha_C$ and $TMP_a$ were similar to the ones observed by Jørgensen et al. [21] in aerobic MBRs.

Figure 2 shows how the model evolved in comparison with the experimental data. Figure 2a shows the applied $J_{20}$, the measured TMP and the modelled TMP in a flux-step trial conducted at a BRF of 7 $Nm^3\ h^{-1}$ (which corresponds to a $BRF_V$ of 0.0032 $Nm^3\ h^{-1}\ m^{-3}$) and a MLTS of 28.5 g $L^{-1}$. Figure 2b shows the modelling results for $\omega_C$ and $R_C$ in the same trial. The results obtained (see Figure 2a) indicated that the results predicted by the model ($TMP_{SIM}$) accurately reproduced the corresponding experimental data ($TMP_{EXP}$): an accurate correlation coefficient ($R^2$) of 0.999 was obtained for the flux-step trial shown. Moreover, it was possible to simulate $\omega_C$ and $R_C$ in the short term (see Figure 2b). As Figure 2b shows, $\omega_C$ increased sharply when $J_{20}$ climbed above 8 LMH, i.e. $\omega_C$ increased from approx. 0.01 to 0.03 kg $m^{-2}$ when $J_{20}$ increased from approx. 8 to 10 LMH. Moreover, $\omega_C$ climbed to 0.06 kg $m^{-2}$ when operating at a $J_{20}$ of approx. 12 LMH, an indication that the critical flux had been exceeded. Figure 2b also shows that $R_C$ increased as $J_{20}$ increased. This is the result of not only the effect of $J_{20}$ on $\omega_C$ (a direct increase in $J_{20}$ means an increase in $\omega_C$ at given operating conditions), but also the effect of TMP on $\alpha_C$ (increasing TMP results in an increase in $\alpha_C$, see Eq. 9 and Eq. 10).

It is important to emphasise that modelling $\omega_C$ and $R_C$ performance may allow the overall performance of membranes in SAnMBR technology to be optimised. In this respect, operating and control strategies aimed to minimise the formation of a cake layer should be tested and developed.

*4.3. Parameter estimations using experimental data and long-term dynamic calibration*

The parameters $K_{S,\mathrm{Xm_c}}$, $k_{RI}$, and $q_{\mathrm{IF,Max}}$ were estimated using experimental data and then validated dynamically using long-term data.

The half-saturation coefficient for the mass of cake solids during membrane scouring and back-flushing ($K_{S,\mathrm{Xm_c}}$) was estimated using experimental data obtained from different short-term trials [18]. The estimated value is shown in Table 4.

The parameter $k_{RI}$ was calculated using data from flux-step trials carried out at different operating times. These flux-step trials resulted in different $\gamma_t$ values. On the other hand, the $R_I$ of each operating time was estimated using data from back-flushing stages (considering $R_M$ to be constant) as shown in Robles et al. [30]. Finally, $k_{RI}$ was calculated, the result being $1.6\cdot10^{-07}$ (see Table 4).

As regards the maximum irreversible fouling rate, since the operating temperature during the operating period was 20 ºC (commonly assumed to be the benchmark temperature when calibrating model parameters) $q_{\mathrm{IF,Max}}$ was directly set as the inverse of the operating SRT (38.5 days in this period): $3\cdot10^{-07}$ $s^{-1}$ (see Table 4). Nevertheless, further study of the long-term data is required in order to determine the actual dependence of $q_{\mathrm{IF,Max}}$ on T and SRT.

*4.4. Default values*

Due to the lack of data, a default value was set for $q_{BF,Max}$, $k_t$ and $\alpha_I$ (see Table 4). As regards $q_{BF,Max}$ and $k_t$, no significant differences were observed in the dynamic calibration when modifying the established default value. Nevertheless, these parameters were included in the model proposed by Sarioglu et al. [17] and Bugge et al. [20]. As regards $\alpha_I$, it may be necessary to calibrate $\alpha_I$ using the experimental data of $R_I$ and $\omega_I$.

**5. Validation of model**

The model was validated in both the short and the long term. The short-term validation consisted of 24 hours of continuous operation. The long-term validation consisted of a 3-month operating period.

*5.1. Short-term validation*

Figures 3 and 4 provide an example of the results obtained from the short-term validation (recorded on operating day 167 in Figure 5). This validation was carried out using experimental data obtained by applying different $J_{20}$ and BRF values. The results shown in Figures 3 and 4 were obtained when operating with a MLTS concentration of 21 g $L^{-1}$. The gas sparging intensity ranged from approx. 4 to 12 $Nm^3\ h^{-1}$. The gross $J_{20}$ ranged from approx. 4 to 12 LMH.

Figure 3a shows the evolution of the experimental $J_{20}$ and BRF. Figure 3b shows the evolution of $TMP_{SIM}$ and $TMP_{EXP}$, and the membrane operating stage. Like Figure

2, Figure 3b shows that although considerably high variations were applied to $J_{20}$ and BRF (see Figure 3a), the results predicted by the model ($TMP_{SIM}$) accurately reproduced the corresponding experimental data ($TMP_{EXP}$) giving a $R^2$ coefficient of 0.962. On the other hand, Figure 3b shows that the model is capable of reproducing the reduction in TMP caused by ventilation or back-flushing (see, for example, minutes 285 and 515, respectively). This model is able to reproduce this reduction in TMP because it takes into account not only the cake build-up, membrane scouring and back-flushing processes, but also the cake compression process. In this respect, a recovery of $\alpha_C$ after each decompression (i.e. relaxation and back-flushing) is achieved. Therefore, a considerable decrease in TMP is observed (see minutes 285 and 515 in Figure 3b) even when operating at low $\omega_C$ levels (see minutes 200 to 600 in Figure 4a).

Figure 4 shows the evolution of the simulated $\omega_C$ and $R_C$ (Figures 4a and 5b, respectively). As figure 4 shows, a sharp increase in both $\omega_C$ and $R_C$ was observed when operating at fluxes close to the critical flux recorded in experiments. Previous trials revealed critical fluxes around operating day 167 of about 8 LMH when operating at a MLTS of 21 g $L^{-1}$ and a BRF of 10 $Nm^3$ $h^{-1}$. These results are in line with the results shown in Figure 4, where a sharp increase in $\omega_C$ was observed (see minutes 600 to 800) when operating at fluxes close to the critical flux.

Figure 4a also shows a minimum amount of $\omega_C$ of about 0.005 kg $m^{-2}$ remaining over time. This performance (modelled mainly by applying the half-saturation switching function represented by Eq. 14) is the result of the drop in the effectiveness of the membrane scouring due to the reduction in the membrane area that is reversibly fouled. This remaining $\omega_C$ was assumed in our study to be one of the main factors that finally determines the propensity of membranes to foul irreversibly. Therefore, in accordance with the sub-critical filtration theory, higher $\omega_C$ values resulting from operating at a high $J_{20}$ will result in a greater propensity to foul irreversibly than when operating at a low $J_{20}$.

On the other hand, sub-critical fouling has been modelled by the increase in the $\alpha_C$ value resulting from applying Eq. 12. In this regard, Figure 4b shows how $R_C$ increases during sub-critical filtration (see, for example, minutes 200 to 600) due to increasing $\alpha_C$. Nevertheless, as mentioned before, $\alpha_C$ returns to its default value when there is no compression of the cake layer, and therefore $R_C$ decreases (see, for example, minutes 285 and 515 in Figure 4b). In our study, a constant sub-critical fouling velocity ($k_{SF}$ in Eq. 12) was established for simulating the sub-critical fouling processes related to specific mechanisms not contemplated in the model. However, this parameter might be established in accordance with the operating value of $J_{20}$ because sub-critical fouling also depends on $J_{20}$.

*5.2. Long-term validation*

The proposed model was validated using the long-term data of the following average daily operating conditions: MLTS levels from approx. 15 – 25 g $L^{-1}$, BRF from 6 to 12 $Nm^3$ $h^{-1}$ and net 20 ºC-normalised transmembrane fluxes ($J_{20net}$) from 2.5 to 9 LMH.

Figure 5 shows the results from the long-term model validation carried out using data from three months of continuous operation. Figure 5a shows the average daily values for $J_{20net}$, BRF, and MLTS. It is important to note that the model was calibrated and validated using highly fouled membranes, which resulted in very low operating

$J_{20net}$ values. Figure 5b shows the average daily $TMP_{SIM}$ and $TMP_{EXP}$. As Figure 5 shows, even when operating at different MLTS, $J_{20net}$ and BRF levels (see Figure 5a), the model was able to accurately predict the membrane performance in the long term (see Figure 5b): a high $R^2$ coefficient was obtained (0.929).

### *5.3. Model applicability and future perspectives*

The model validation shown in this study illustrates that the proposed model was able to properly reproduce the filtration performance of an SAnMBR system in the short- and long-term. Moreover, a sensitivity analysis based on the Morris method [31] revealed that most of the suggested model parameters were identified as influential (data not shown). This was mainly the result of building the model on the basis of experimental results. Therefore, most of the proposed model parameters are required to represent in a general way all possible membrane performances in systems of this type. The less influential parameters were: $K_{S,XmC}$, $q_{IF,Max}$, $\alpha_I$, $q_{BF,Max}$ and $k_t$, which implies that these parameters could be set to a default value in order to simplify the model calibration.

It is worth to point out that some estimations/measurements (e.g. cake and irreversible fouling thickness and specific resistance) would further improve process validation for accurately validating not only the modelling approach but also the calibrated values for the different model parameters. Therefore, further research would be required on this area.

On the other hand, further research must be accomplished in order to extend the applicability of the proposed filtration model to other MBR applications (e.g. aerobic operation, flat-sheet membrane modules, industrial wastewater treatment, and so on.). To this aim, it is expected that the re-calibration of the model parameters would be necessary. In this regard, recent literature reveals differences on membrane performance in MBR technology not only due to changes on the physiological state of the mixed liquor but also due to changes on membrane operating mode and configuration [18]. Nevertheless, it is important to highlight the wide range of operating conditions in which the model has been validated in this work: influent COD concentration from approx. 200 to 900 mgCOD $L^{-1}$, MLTS levels from approx. 15 – 25 g $L^{-1}$, BRF from 6 to 12 $Nm^3$ $h^{-1}$ and $J_{20net}$ from 2.5 to 9 LMH.

In the future, it is planned to validate this model at a wider range of operating conditions, mainly regarding membrane operating mode and mixed liquor characteristics. Moreover, it is planned to verify the applicability of the model for other membrane module configurations such as flat-sheet type. Then, the corresponding model modifications will be made if necessary, in order to verify and/or extend the applicability of the proposed model, which will facilitate the design and simulation of membrane technology in WWTPs.

Other aspect on filtration process to be considered is that biological modelling on anaerobic filtration-based systems is quite recent, which makes difficult to obtain reliable information about the interaction between biological and filtration processes. In this respect, enhancing biological modelling of anaerobic processes of this type may allow improving the quality of the proposed filtration model since a greater amount of reliable data related to different fouling mechanisms (e.g. EPS, SMP, colloidal matter, etc.) would be available.

Finally, it must be highlighted that the proposed filtration model (in conjunction with a biological model) can be applied for different reasons: to design and upgrade SAnMBR systems, or to develop, operate and control strategies designed to optimise process performance – not only in the short term, but also in the long term.

## 5. Conclusions

The short- and long-term validation of the filtration model proposed in this study resulted in satisfactory correlation coefficients ($R^2$) of 0.962 and 0.929 respectively. Thus, this model was able to accurately reproduce the filtration process in a SAnMBR demonstration plant fitted with industrial-scale hollow-fibre membranes. This model can be used to develop operating and control strategies intended to optimise filtration in SAnMBRs since the weighted average distribution of overall filtration resistance can be modelled. Further research will be done in order to extend the applicability of the proposed filtration model to a wider range of operating conditions and other MBR applications.

## Acknowledgements

This research has been supported by the Spanish Ministry of Economy and Competitiveness (MINECO Project CTM2011-28595-C02-01/02) jointly with the European Regional Development Fund (ERDF), which are gratefully acknowledged.

## References

[1] G. Mannina, G. Di Bella, G. Viviani, An integrated model for biological and physical process

simulation in membrane bioreactors (MBRs), J. Membrane Sci. 376 (2011), 56 – 69.

[2] A.N.L. Ng, A.S. Kim, A mini-review of modeling studies on membrane bioreactor (MBR) treatment for municipal wastewaters, Desalination 212 (2007), 261 – 281.

[3] M. Henze, W. Gujer, T. Mino, M.C.M. van Loosdrecht, Activated Sludge Models: ASM1, ASM2, ASM2d and ASM3, Scientific and Technical Report no. 9, IWA Publishing, London, UK, 2000.

[4] D.J. Batstone, J. Keller, I. Angelidaki, S.V. Kalyuzhnyi, S.G. Pavlostathis, A. Rozzi, W.T. Sanders, H. Siegrist, V.A. Vavilin, The IWA anaerobic digestion model No. 1 (ADM1), Water Sci. Technol. 45 (2002), 65 – 73.

[5] M. de Gracia, P. Grau, E. Huete, J. Gómez, J.L. García-Heras, E. Ayesa, New generic mathematical model for WWTP sludge digesters operating under aerobic and anaerobic conditions: Model building and experimental verification. Water Res. 43 (2009), 4626 – 4642.

[6] R. Barat, J. Serralta, M.V. Ruano, E. Jiménez, J. Ribes, A. Seco, J. Ferrer, Biological Nutrient Removal Model Nº 2 (BNRM2): A general model for Wastewater Treatment Plants, Water Sci. Technol. (2012), http://dx.doi.org/10.2166/wst.2013.004.

[7] W. Naessens, T. Maere, I. Nopens, Critical review of membrane bioreactor models – Part 1: Biokinetic and filtration models, Bioresour. Technol. 122 (2012) 95 – 106.

[8] W. Naessens, T. Maere, N. Ratkovich, S. Vedantam, I. Nopens, Critical review of membrane bioreactor models – Part 2: Hydrodynamic and integrated models, Bioresour. Technol. 122 (2012) 107 – 118.

[9] M.F.R. Zuthi, H.H. Ngo, W.S. Guo, Modelling bioprocesses and membrane fouling in membrane bioreactor (MBR): A review towards finding an integrated model framework, Bioresour. Technol. 122 (2012) 119 – 129.

[10] A. Broekmann, J. Busch, T. Wintgens, W. Marquardt, Modeling of pore blocking and cake layer formation in membrane filtration for wastewater treatment, Desalination 189 (2006), 97 – 109.

[11] C. Duclos-Orsello, W. Li, C.C. Ho, A three mechanism model to describe fouling of microfiltration membranes, J. Membrane Sci. 280 (2006), 856 – 866.

[12] X.y. Li, X.m. Wang, Modelling of membrane fouling in a submerged membrane bioreactor, J. Membrane Sci. 278 (2006), 151 – 161.

[13] J. Busch, A. Cruse, W. Marquardt, Modeling submerged hollow-fiber membrane filtration for wastewater treatment, J. Membrane Sci. 288 (2007), 94 – 111.

[14] A. Zarragoitia-Gonzalez, S. Schetrite, M. Alliet, U. Jauregui-Haza, C. Albasi, Modelling of

submerged membrane bioreactor: Conceptual study about link between activated sludge biokinetics, aeration and fouling process, J. Membrane Sci. 325 (2008), 612 – 624.

[15] J. Wu, C. He, Y. Zhang, Modeling membrane fouling in a submerged membrane bioreactor by considering the role of solid, colloidal and soluble components, J. Membrane Sci. 397/ 398 (2012), 102–111.

[16] T. Ludwig, D. Gaida, C. Keysers, J. Pinnekamp, M. Bongards, P. Kern, C. Wolf, A.L. Sousa Brito, An advanced simulation model for membrane bioreactors: Development, Calibration and Validation, In: 6th IWA Specialist Conference on Membrane Technology for Water & Wastewater Treatment, 2011.

[17] M. Sarioglu, G. Insel, D. Orhon, Dynamic in-series resistance modeling and analysis of a submerged membrane bioreactor using a novel filtration mode, Desalination 285 (2012), 285 – 294.

[18] A. Robles, M.V. Ruano, J. Ribes, J. Ferrer, Factors that affect the permeability of commercial hollow-fibre membranes in a submerged anaerobic MBR (HF-SAnMBR) system, Water Res. 47 (2013), 1277 – 1288.

[19] American Public Health Association/American Water Works Association/Water Environmental Federation, Standard methods for the Examination of Water and Wastewater, 21st edition, Washington DC, USA, 2005.

[20] T.V. Bugge, M.K. Jørgensen, M.L. Christensen, K. Keiding, Modeling cake buildup under TMP-step filtration in a membrane bioreactor: Cake compressibility is significant, Water Res. 46 (2012), 4330 – 4338.

[21] M.K. Jørgensen, T.V. Bugge, M.L. Christensen, K. Keiding, Modeling approach to determine cake buildup and compression in a high-shear membrane bioreactor, J. Membrane Sci. 409/410 (2012), 335 – 345.

[22] T.F. Coleman, Y. Li, An interior, trust region approach for nonlinear minimization subject to bounds. SIAM J. Optim. 6 (1996), 418 – 445.

[23] M.L. Christensen, The Effect of Filter Cake Viscoelasticity on Filtration: a Study of Activated Sludge Dewatering, PhD thesis, Aalborg University, Department of Biotechnology, Chemistry and Environmental Engineering, Aalborg, Denmark, 2006.

[24] LD. Hughes, R.W. Field, Crossflow filtration of washed and unwashed yeast suspensions at constant shear under nominally sub-critical conditions, J. Membr. Sci. 280 (2006), 89 – 98.

[25] L. Corominas, L. Rieger, I. Takács, G. Ekama, H. Hauduc, P.A. Vanrolleghem, A. Oehmen, K.V. Gernaey, M.C.M. van Loosdrecht, Y. Comeau, New framework for standardized notation in wastewater

treatment modelling, Water Sci. Technol. 61 (2010), 841 – 857.

[26] A. Robles, M.V. Ruano, F. García-Usach, J. Ferrer, Sub-critical filtration conditions of commercial hollow-fibre membranes in a submerged anaerobic MBR (HF-SAnMBR) system: The effect of gas sparging intensity, Bioresour. Technol. 114 (2012), 247 – 254.

[27] P. Le-Clech, V. Chen, T.A.G. Fane, Fouling in membrane bioreactors used in wastewater treatment, J. Membr. Sci. 284 (2006), 17 – 53.

[28] A. Robles, M.V. Ruano, J. Ribes, J. Ferrer, Performance of industrial scale hollow-fibre membranes in a submerged anaerobic MBR (HF-SAnMBR) system at mesophilic and psychrophilic conditions, Sep. Purif. Technol. 104 (2013), 290 – 296.

[29] F.G. Meng, S.R. Chae, A. Drews, M. Kraume, H.S. Shin, F.L. Yang, Recent advances in membrane bioreactors (MBRs): membrane fouling and membrane materials, Water Res. 43 (2009), 2405 – 2415.

[30] A. Robles, M.V. Ruano, J. Ribes, J. Ferrer, Advanced control system for optimal filtration in submerged anaerobic MBRs (SAnMBRs), J. Membrane Sci. 430 (2013), 330 – 341.

[31] M. Morris, Factorial sampling plans for preliminary computational experiments, Technometrics. 33 (1991), 239 – 245.

## Figure and table captions

**Figure 1.** Effect of $J_{20}$ on FR when operating at $BRF_V$ of 0.0023, 0.0032 and 0.0046 $Nm^3\ h^{-1}\ m^{-3}$, and MLTS of **(a)** 18.5, **(b)** 22.5, and **(c)** 28.5 g $L^{-1}$.

**Figure 2.** Results of the dynamic calibration of $q_{MS,Max}$, $k_{SF}$, $\alpha_{C,0}$, and $TMP_a$. Flux-step experiment conducted at a MLTS of 28.5 g $L^{-1}$ and a BRF of 7 $Nm^3\ h^{-1}$. Evolution of **(a)** $TMP_{EXP}$, $TMP_{SIM}$ and $J_{20}$ and **(b)** $\omega_C$ and $R_C$.

**Figure 3.** Short-term model validation: results from operating day 167 (see Figure 5). Evolution of **(a)** $J_{20}$ and BRF and **(b)** $TMP_{EXP}$, $TMP_{SIM}$ and membrane operating stage (V:Ventilation; BF:Back-Flushing).

**Figure 4.** Short-term model validation: results from operating day 167 (see Figure 5).

Evolution of **(a)** $\omega_C$ and **(b)** $R_C$.

**Figure 5.** Long-term model validation. Average daily values of **(a)** MLTS, $J_{20}$ and BRF and **(b)** $TMP_{EXP}$ and $TMP_{SIM}$.

**Table 1.** Stoichiometry of the kinetic processes contemplated in the model.

**Table 2**. Conversion factors to be applied in the continuity equations of the mass of the model.

**Table 3.** Kinetic expressions of the processes included in the model.

**Table 4.** Values assumed for the different parameters included in the proposed filtration model.

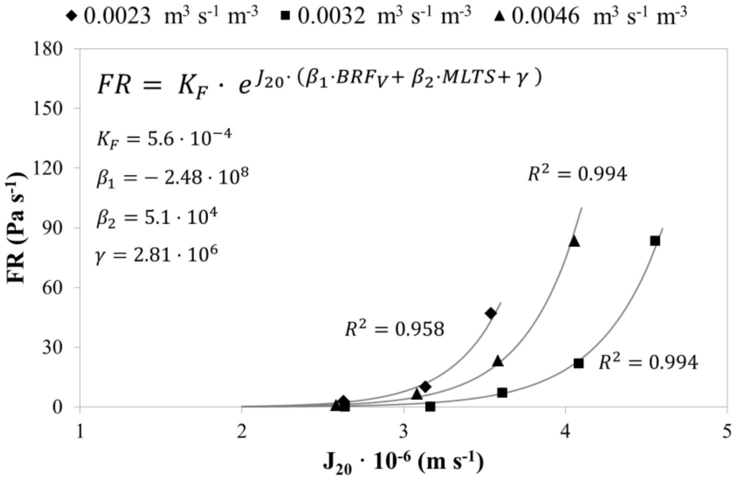


**(a)**

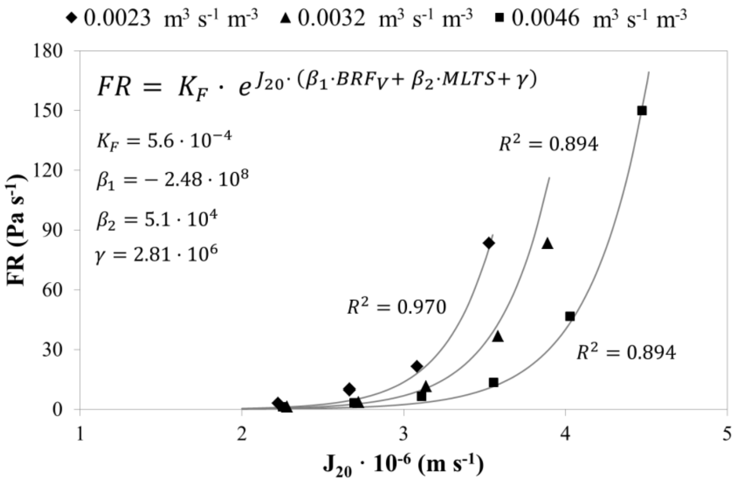


**(b)**

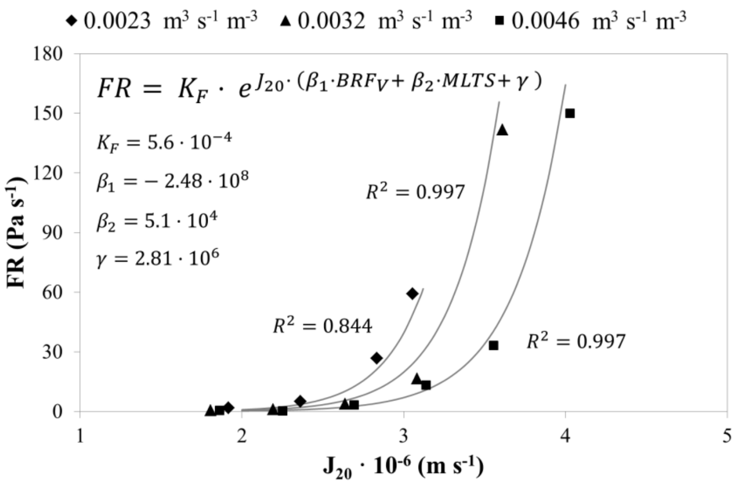


**(c)**

**Figure 1.** Effect of $J_{20}$ on FR when operating at $BRF_V$ of 0.0023, 0.0032 and 0.0046 $Nm^3\ h^{-1}\ m^{-3}$, and MLTS of **(a)** 18.5, **(b)** 22.5, and **(c)** 28.5 g $L^{-1}$.

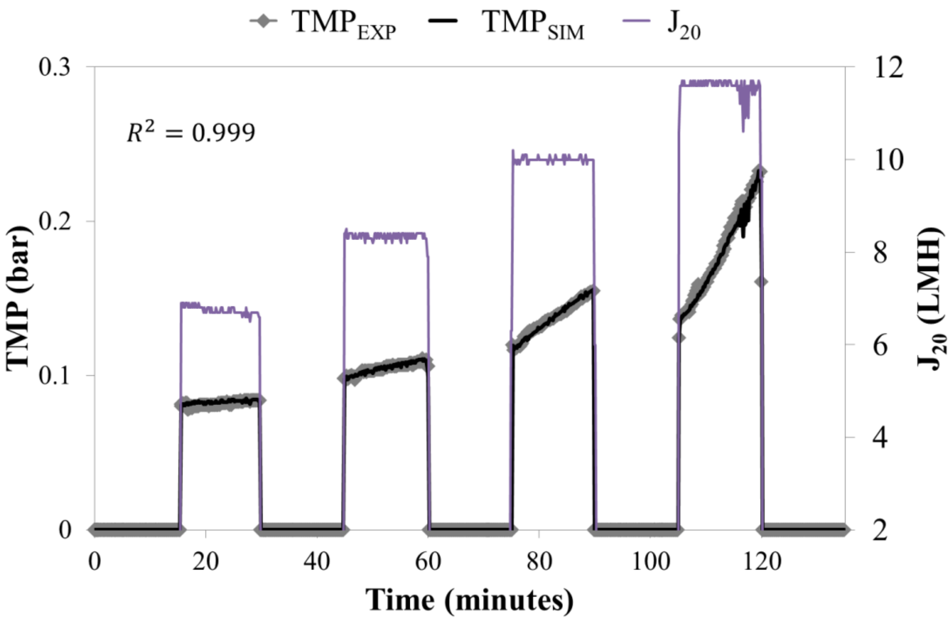


**(a)**

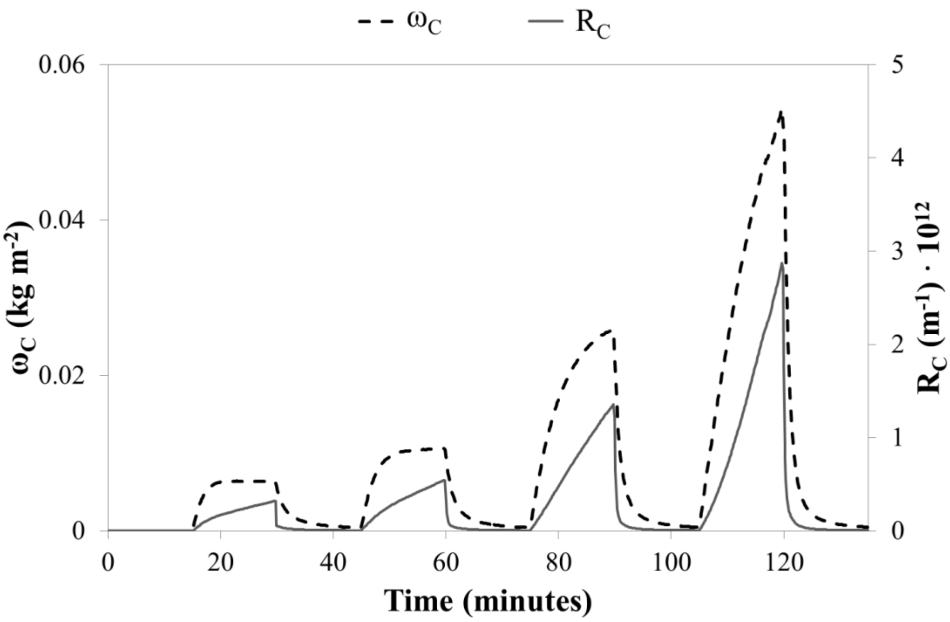


**(b)**

**Figure 2.** Results of the dynamic calibration of $q_{\mathrm{MS,Max}}$, $k_{SF}$, $\alpha_{C,0}$, and $TMP_a$. Flux-step experiment conducted at a MLTS of 28.5 g $L^{-1}$ and a BRF of 7 $Nm^3\ h^{-1}$. Evolution of **(a)** $TMP_{EXP}$, $TMP_{SIM}$ and $J_{20}$ and **(b)** $\omega_C$ and $R_C$.

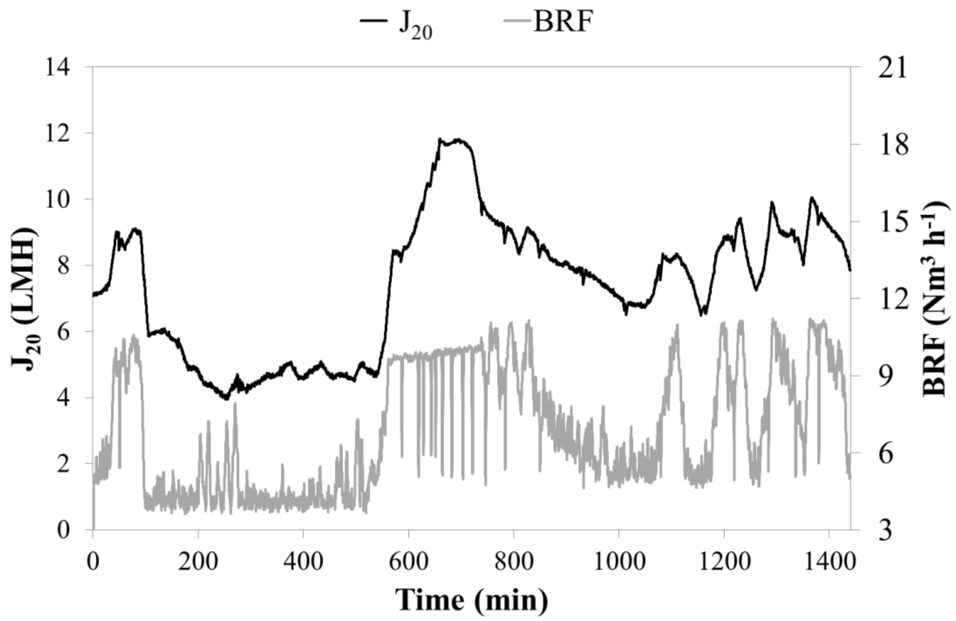


(a)

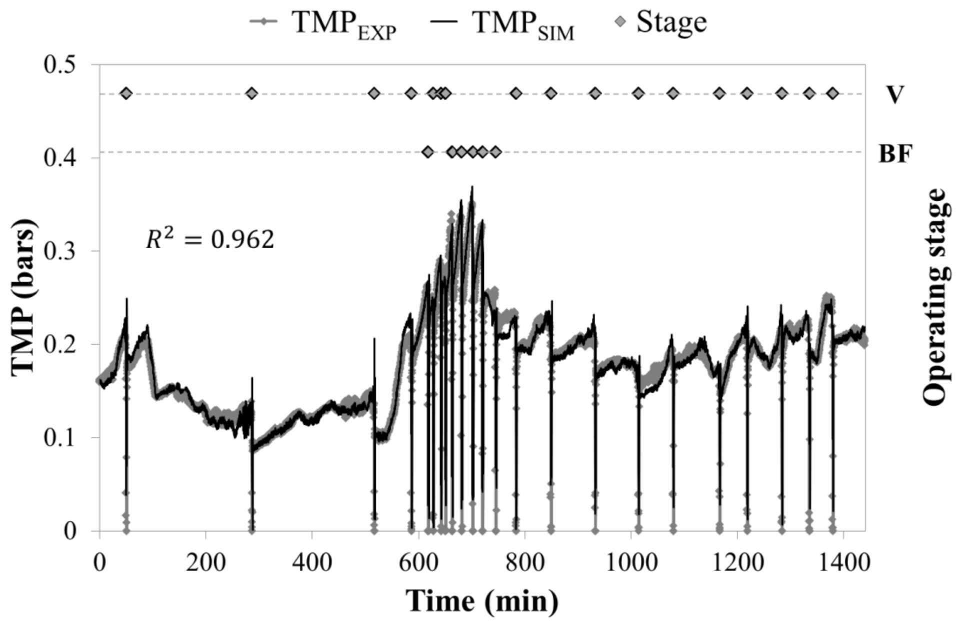


(b)

**Figure 3.** Short-term model validation: results from operating day 167 (see Figure 5). Evolution of **(a)** $J_{20}$ and BRF and **(b)** $TMP_{EXP}$, $TMP_{SIM}$ and membrane operating stage (V:Ventilation; BF:Back-Flushing).

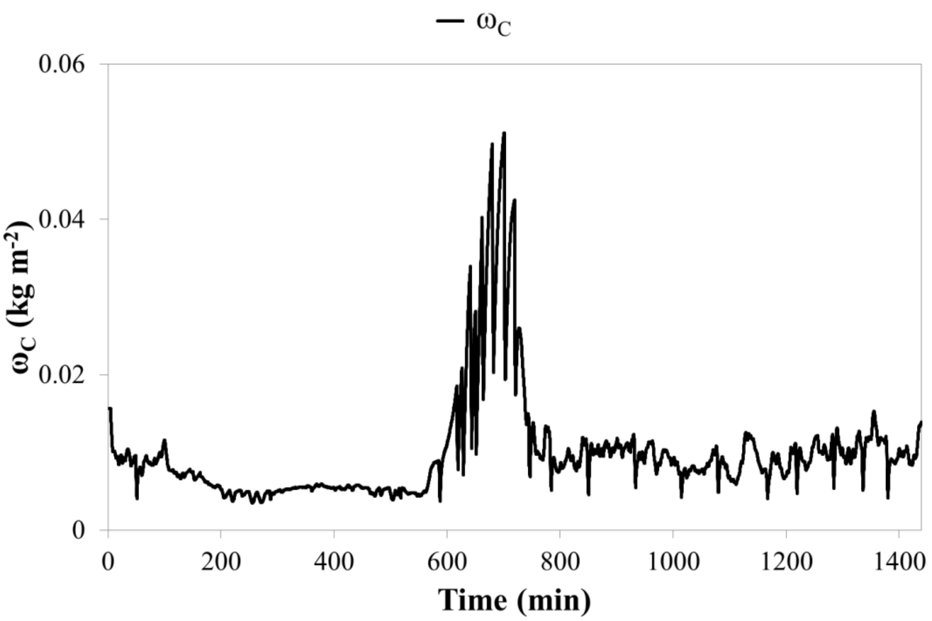


**(a)**

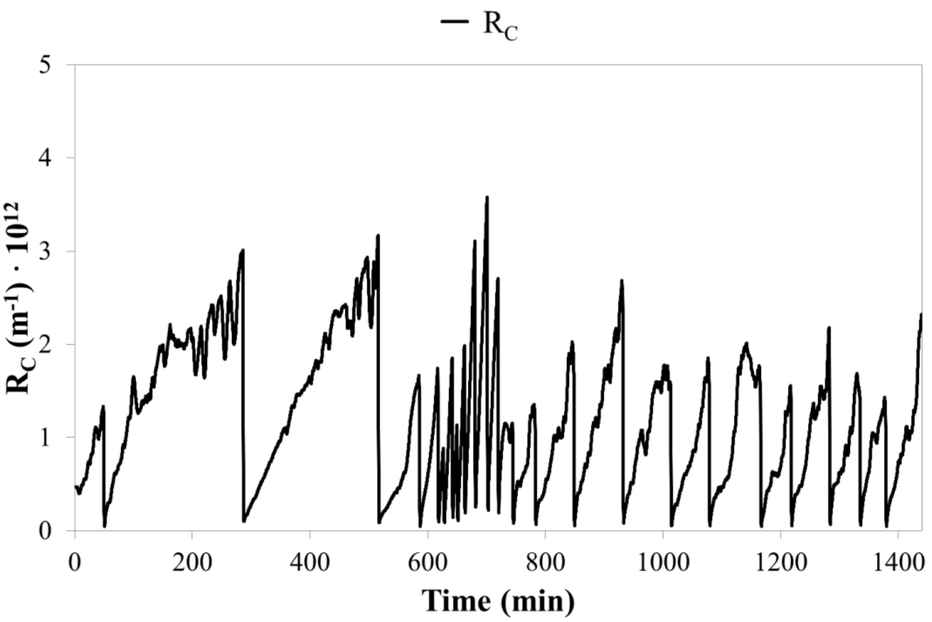


**(b)**

**Figure 4.** Short-term model validation: results from operating day 167 (see Figure 5).

Evolution of **(a)** $\omega_C$ and **(b)** $R_C$.

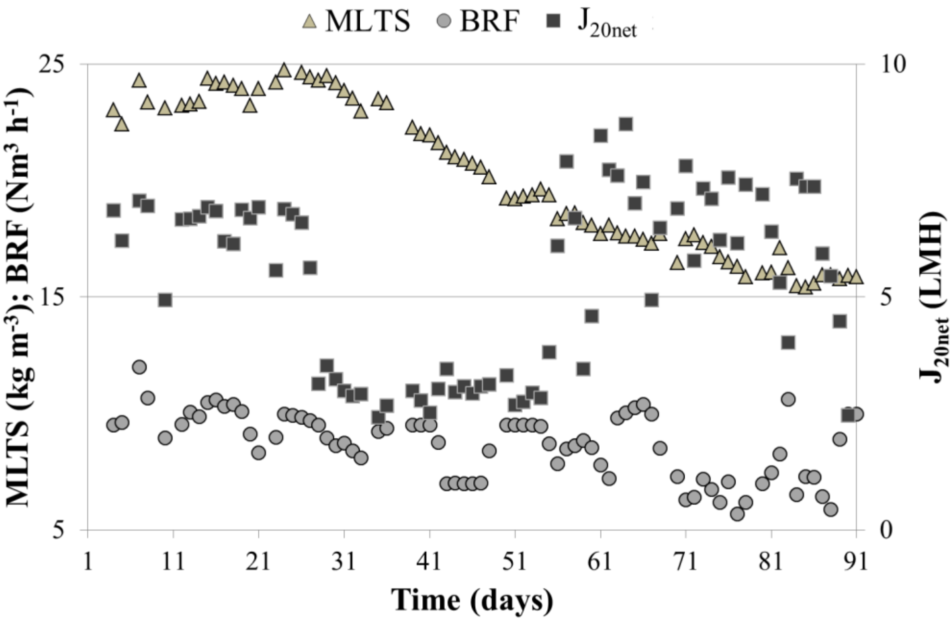


(a)

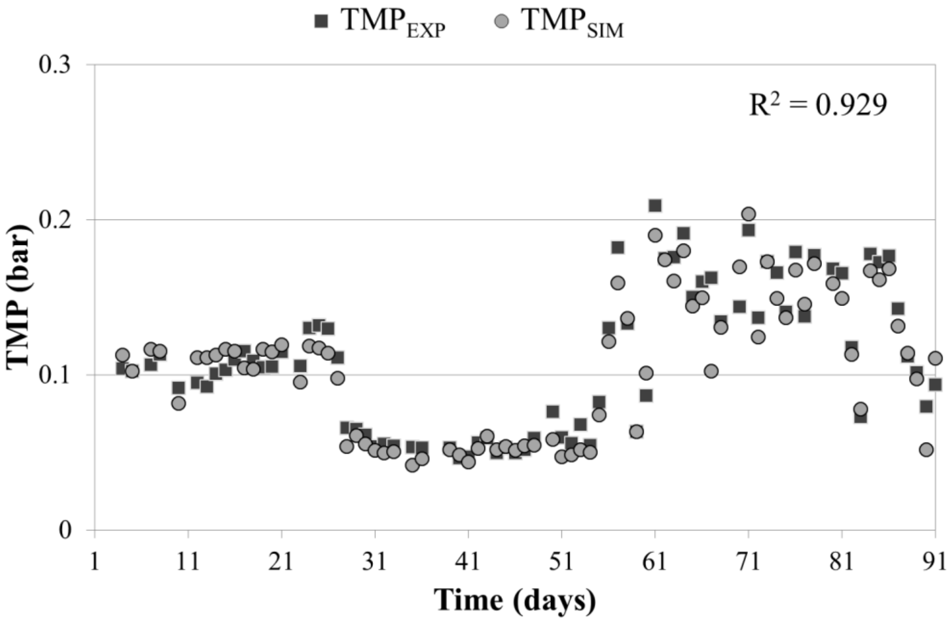


(b)

**Figure 5.** Long-term model validation. Average daily values of **(a)** MLTS, $J_{20}$ and BRF and **(b)** $TMP_{EXP}$ and $TMP_{SIM}$.

**Table 1.** Stoichiometry of the kinetic processes contemplated in the model.

| j Process \ Component i | $X_{TS}$ (kg TS m$^{-3}$) | $X_{m_C}$ (kg TS) | $X_{m_I}$ (kg TS) |
|---|---|---|---|
| 1. Cake layer formation | -1 | 1 | |
| 2. Membrane scouring by biogas sparging | 1 | -1 | |
| 3. Cake layer detachment during back-flushing | 1 | -1 | |
| 4. Irreversible fouling consolidation | | -1 | 1 |

**Table 2**. Conversion factors to be applied in the continuity equations of the mass of the model.

| Conservation for \ Component i | $X_{\mathrm{TS}}$ (kg TS) | $X_{\mathrm{m_C}}$ (kg TS) | $X_{\mathrm{m_I}}$ (kg TS) |
|---|---|---|---|
| Mass (kg TS) $i_{TS\_i}$ | -1 | 1 | 1 |

**Table 3.** Kinetic expressions of the processes included in the model.

| *j Process* | *Kinetic expression* |
|---|---|
| 1. Cake layer formation | $Q_{20P} \cdot X_{\mathrm{TS}}$ |
| 2. Membrane scouring by biogas sparging | $q_{\mathrm{MS,Max}} \cdot M_{X_{\mathrm{m_C}}} \cdot I_{\mathrm{MS}} \cdot BRF_{\mathrm{V}} \cdot X_{\mathrm{m_C}}$ |
| 3. Cake layer detachment during back-flushing | $q_{\mathrm{BF,Max}} \cdot Q_{20BF} \cdot M_{X_{\mathrm{m_C}}} \cdot X_{\mathrm{m_C}}$ |
| 4. Irreversible fouling consolidation | $q_{\mathrm{IF,Max}} \cdot X_{\mathrm{m_C}}$ |

**Table 4.** Values assumed for the different parameters included in the proposed filtration model.

| Parameter | Unit | Value | Calculation method |
|---|---|---|---|
| $q_{\mathrm{MS,Max}}$ | | 6.31 | Dynamically calibrated |
| $q_{\mathrm{BF,Max}}$ | $m^{-3}$ | 1 | Default value |
| $q_{\mathrm{IF,Max}}$ | $s^{-1}$ | $3 \cdot 10^{-07}$ | Calculated from experimental data |
| $K_{S,XmC}$ | kg SST | 0.2 | Calculated from experimental data |
| $\alpha_{C,0}$ | m $kg^{-1}$ | $1.02 \cdot 10^{13}$ | Dynamically calibrated |
| $TMP_a$ | kPa | 18.9 | Dynamically calibrated |
| $k_t$ | $s^{-1}$ | 1 | Default value |
| $k_{SF}$ | m $kg^{-1}$ $s^{-1}$ | $4.09 \cdot 10^{10}$ | Dynamically calibrated |
| $K_F$ | Pa $s^{-1}$ | $5.6 \cdot 10^{-4}$ | Experimentally calibrated |
| $\beta_1$ | $s^2$ $m^{-1}$ | $-2.48 \cdot 10^{8}$ | Experimentally calibrated |
| $\beta_2$ | s $m^2$ $kg^{-1}$ | $5.1 \cdot 10^{4}$ | Experimentally calibrated |
| $\gamma_0$ | s $m^{-1}$ | $2.81 \cdot 10^{6}$ | Experimentally calibrated |
| $k_{RI}$ | s | $1.6 \cdot 10^{-07}$ | Calculated from experimental data |
| $\alpha_I$ | m $kg^{-1}$ | $1 \cdot 10^{14}$ | Default value |